

Compound Finishing of *Bombyx mori* Silk: A Study of Cold Oxygen Plasma/Titania Sols Treatments and Their Influences on Fiber Structure and Performance

Chenghui Zheng · Guoqiang Chen · Zhenming Qi

Received: 17 November 2011 / Accepted: 5 January 2012 / Published online: 1 March 2012
© Springer Science+Business Media, LLC 2012

Abstract Degummed *Bombyx mori* (*B. mori*) silk fabrics modified by cold oxygen plasma (COP) and/or titania sols (TSs) were investigated by Fourier transform infrared spectroscopy (FT-IR), X-ray diffraction, field emission scan electronic microscopy (FE-SEM), thermo-gravimetric and differential thermal analysis, and ultraviolet (UV) transmittance methods in this study. FT-IR analysis demonstrated that titania particles were associated with *B. mori* silk fibers by forming organic–inorganic hybrid blends. Processing sequences of COP and TSs, and curing conditions showed significant impacts on the crystalline, thermal, micro-morphological, and UV resistant characteristics of silk fabrics. Crystallinity index by both area and height methods, and crystallite sizes of silk fabrics were calculated as well. Results showed that crystallinity index of finished samples approximate to that of degummed silk fabric could be obtained by applying TSs and curing at 160 °C for 2 min prior to COP treatment, or vice versa with lower temperature of 140 °C for 3 min, whereas the crystallite sizes of treated samples increased slightly. The initial decomposition temperatures of finished samples were elevated by 23–35 °C with increased char residues at 600 °C, while the transmittance of UVA and UVB of finished samples decreased by 11.7, 17.7%, respectively. FE-SEM analysis revealed that titania particles were associated on the fiber surfaces with different smoothness.

Keywords Cold plasma · Dyes/pigments · Fibers · Gels · Proteins

C. Zheng · G. Chen (✉)
College of Textile and Clothing Engineering,
Soochow University, Suzhou 215006, Jiangsu Province, China
e-mail: chenguojiang@suda.edu.cn

C. Zheng · Z. Qi
School of Textiles and Clothing, Yancheng Institute of Technology, Yancheng 224051,
Jiangsu Province, China

Introduction

For thousands of years, *Bombyx mori* silk fibers have been used as materials of luxury apparels in textile fields for their elegant appearance, good feelings and skin compatibilities, high moisture regain, etc. However, their poor wrinkle recovery abilities, poor anti-microbial abilities, and easy sensibility to ultraviolet radiation in sunshine have greatly restricted their applications in fields such as medical, protective clothes. Many researches have been carried out in improving the end uses of *B. mori* silk fibers in recent years, involving physical or chemical finishing, surface grafting or modifications, regenerated silk fiber, etc. [1, 2]. However, few researches have been focused on compound finishing of *B. mori* silk by combining several different processing methods. As a matter of fact, combinations of different processing methods, compared with the single ones, can obtain more multi-functional fabrics or greatly improve some performance of fabrics such as UV resistance and thermal stabilities.

Plasma technologies have become more and more popular in modifying polymer surfaces in recent years [3, 4], however, the mechanism of interactions between plasma and surfaces is extremely complex and difficult to be clearly understood. Plasma, a matter with a state similar to gas, comprises charged and neutral species presenting mass behavior. These species are mixture of positive ions, negative ions, electrons, radicals, atoms, and excited molecules, etc. When a material is surface modified by plasma, the typical depth of modification is several hundreds of angstroms [5]; mutual interaction between the material surface and active particles occurs because of roles such as plasma ultraviolet radiation, surface etching, cross-linking construction layer, radicals, etc. [6]. Nitrogen, Oxygen, and Argon are often used in cold plasma devices. In case of Oxygen, the following two reactions exist simultaneously [7]: (1) etching of polymer surfaces due to formation of volatile products, which are the results of reaction between oxygen atoms and surface carbon atoms; (2) formation of oxygen-containing functional groups at polymer surfaces due to reactions of active species in plasma and surface atoms. All newly generated radicals can take part in subsequent reactions such as introducing functional groups, forming cross-linking construction, etc. These succeeding reactions are especially important in surface modifications of materials.

Having large specific areas, nano-titania has been widely applied as white pigments, inorganic UV-resistant agents, and anti-microbial agents, etc. in textile industries [8]. Nano-titania can modify the directions of incident UV radiation by scatter or reflect action, avoiding their penetrating through fabrics and hurting human skins. Titania is applied to textiles in the following ways: (1) as filling material of functional fibers; (2) as functional modifiers for fabrics in textile chemical processing [9, 10]. There are several methods to prepare nano-titania such as mechanical grinding, hydrolyzing TiCl_4 in vapor phase, sol-gel processes, etc. [11]. A sol-gel process starts from a metal alkoxides or some inorganic salts (e.g. nitrates, acetates, chlorides), namely the precursor, which undergoes a series of hydrolysis and polycondensations in solution, concludes when the sol turns into a gel. When dried and annealed at high temperature, the gel results metal oxides of nanometer scale. The reacting conditions are relatively mild and easy controlled with high pure products, whereas the high costs of precursors and poor sintering abilities of gels have greatly hindered the massive application.

In order to investigate the morphological, structural, thermal, and UV resistant abilities of *B. mori* fabrics finished by cold oxygen plasma (COP)/titania sols (TSs), we have prepared TSs by sol-gel methods and applied the sols with or without COP on degummed

B. mori silk fabrics. Processing sequences, curing conditions, etc. are also to be examined in this study.

Experimental

Materials

Plain *B. mori* silk fabrics (25.0 g m^{-2} , $380 \text{ yarns dm}^{-1}$ both warp and weft directions, from Huzhou silk factory, Huzhou, China) were degummed twice with 0.5 wt% sodium carbonate at 95°C for 30 min for fully removal of sericin, then rinsed with deionized water and dried at ambient temperature.

Tetrabutylorthotitanate (TOBT, $\text{Ti}(\text{OC}_4\text{H}_9)_4$) and bis(P,P-bis-ethylhexyldiphosphato) ethanediolatitanate (BPET, $\text{C}_{34}\text{H}_{74}\text{O}_{16}\text{P}_4\text{Ti}$) were chemically pure and purchased from Nanjing Pinning Coupling Agents Co., Ltd, Nanjing, China; ethanol, 37% hydrochloric acid, sodium carbonate etc. were all analytical grade without any further purification in this study.

Preparation of TSs

Mixture of 2.8385×10^{-3} mol TOBT and 7.1154×10^{-4} mol BPET ($n_{[\text{BPET}]}:n_{[\text{TOBT}]} = 1:4$, in mole ratio, similarly hereinafter) was dripped into 2/3 parts of ethanol ($n_{[\text{Ti}]}:n_{[\text{EtOH}]} = 1:30$), after a vortex of 5 min, the transparent, yellowish solution, namely A, would appear; A certain amount of deionized water, 4.8252×10^{-4} mol hydrochloric acid, 1/3 part of ethanol were mixed, resulting another solution, namely B. Afterwards, solution B was added into solution A, and the mixture underwent 5-minutes' vortex, obtaining a dilute, yellowish titania sol. Generally, only sols can be used to finish fabrics and they should be relatively stable, which means gels will not occur in scores of hours or even longer in storage in the study. The median diameter of titania particles in the sol was about 72.8 nm with polydispersity index (P.I.) of 0.629 according to our previous studies [12].

Application of TSs

Each of 0.4 g *B. mori* silk fabrics was immersed into the as-prepared, individual titania sol (Counting as Ti^{4+} , $0.4426 \text{ mol L}^{-1}$) and was treated in ultrasonic cleaner (Model KQ5200DB, Kunshan Ultrasonic Instruments Co., Ltd, Kunshan, China) at 20°C for 30 min. The samples were taken out, squeezed to wet pickup of 200 wt%, dried at 80°C for 5 min, then cured on M-6 pin tenter (Nantong Baolai Textile Equipment Co., Ltd., Nantong, China) at $140\text{--}170^\circ\text{C}$ for 1–3 min. Finally the samples were rinsed with deionized water of 60°C thoroughly, taken out and dried at ambient temperature for further uses.

COP Treatment of Fabrics

Bombyx mori silk fabrics were hung in the cylindrical chamber of cold plasma equipment (Model HD-1B, Changzhou Zhongke Changtai Plasma Technology Co., Ltd, Changzhou, China) and underwent 3 min plasma treatment. The pressure of oxygen was maintained at 10 Pa, with power of 100 Watt.

Characterization

FT-IR

Nexus-6700 Fourier transform infrared spectrometer (FT-IR, Thermo Fisher Scientific Inc., Waltham, MA, USA) was used to evaluate the infrared absorbing abilities of silk fabrics. Samples were cut into fine powder and ground with potassium bromide (KBr) to make discs.

X-ray Diffraction

The X-ray diffraction (XRD) patterns of silk fabric powder were obtained from X'Pert Pro MPD—multipurpose X-ray diffractometer (The Analytical X-ray Company, PANalytical B.V., ALMELO, The Netherlands), which was equipped with Ni-filtered $\text{CuK}\alpha$ radiation generated at a voltage of 40 kV and current of 150 mA. The scanning speed was 5° min^{-1} within range of $5\text{--}50^\circ$. All curves were deconvoluted with peakfit software (Version 4.12, Galactic Industries Corporation, New Hampshire, USA). The calculating methods of crystallinity index (C.I.) of silk fibers by area or height were illustrated in Scheme 1, and Eqs. 1 and 2 were also listed as follows [13, 14]:

$$\text{Area : C.I.(\%)} = \frac{A_c}{A_c + A_a} \times 100 \quad (1)$$

$$\text{Height : C.I.(\%)} = \frac{h_c}{h_t} \times 100 \quad (2)$$

where A_c = Area of all crystalline regions

A_a = Area of all amorphous regions

h_c = height of main crystalline peak

h_t = total height of main crystalline peak

Crystallite sizes of silk fibers were calculated according to the well-known Scherrer equation (see Eq. 3):

$$D = \frac{K\lambda}{\cos \theta \cdot FWHM} \quad (3)$$

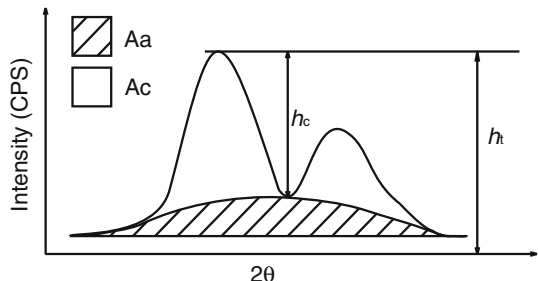
where: D : crystallite size vertically to corresponding lattice plane (nm)

K : form factor (0.89–1.39), here $K = 0.89$

λ : wave length of $\text{CuK}\alpha$ radiation (nm) ($\lambda = 0.1542 \text{ nm}$)

θ : angle of incidence (rad)

Scheme 1 Calculation of crystallinity index. A Area; h height; c crystalline region; a amorphous region



FWHM Full width at half maximum peak intensity (rad), obtained from analyzing the Gaussian distribution in the deconvolution of the crystalline peaks in peakfit software.

Scanning Electron Microscopy

High resolution cold field emission scanning electron microscope (FE-SEM, Hitachi S-4800, Hitachi High-Technologies Corporation, Tokyo, Japan) was used to investigate the areal microstructural morphology of samples. The accelerating voltages were 3–5 kV.

Thermo-Gravimetric and Differential Thermal Analysis

Thermal characteristics of both finished and unfinished samples were investigated by Thermo-Gravimetric and Differential Thermal Analyzer Pyris Diamond TG-DTA, Perkin Elmer Inc., Waltham, Massachusetts, USA). All scans were carried out at a heating rate of $10\text{ }^{\circ}\text{C min}^{-1}$ at a temperature ranged from ambient temperature to $600\text{ }^{\circ}\text{C}$ under flowing nitrogen at flow rate of 20 mL min^{-1} . Samples weighing about 0.3 mg were cut into powder and placed into the standard pans for determination of their thermal properties.

UV Transmittance

Ultraviolet transmittance of both finished and unfinished dry *B. mori* silk fabrics were measured on Model YG(B) 912E textile UV-resistant performance tester (Wenzhou Darong Textile Instruments Co., Ltd., Wenzhou, China) according to American Association of Textile Chemists and Colorists (AATCC) test method-183. Transmittance data of UVA (320–400 nm) and UVB (280–320 nm) were recorded.

Results and Discussion

FT-IR Analysis

Figure 1 shows the FT-IR spectra of degummed (Fig. 1a), COP treated (Fig. 1b) and TS/COP treated (Fig. 1c, d, e, f) silk fabrics. The broad absorption band centered at $3,291\text{ cm}^{-1}$ is attributed to stretching vibration of molecular water and hydroxyl groups. $2,973\text{ cm}^{-1}$ and $2,869\text{ cm}^{-1}$, respectively correspond to the asymmetric and symmetric CH_3 stretching vibration from silk, while $2,927\text{ cm}^{-1}$ corresponds to the asymmetric stretching vibration of CH_2 . The strong peak around $1,703\text{ cm}^{-1}$ is due to $\text{C}=\text{O}$ stretching vibration. In general, the amide I mode associated with α -helical conformation occurs in the range of $1,650\text{--}1,660\text{ cm}^{-1}$, the random coil conformation gives band in the range of $1,640\text{--}1,650\text{ cm}^{-1}$, the β -sheet conformation results in the band between $1,620\text{ cm}^{-1}$ and $1,640\text{ cm}^{-1}$ [15, 16]. The variety of peaks near 995 cm^{-1} and 967 cm^{-1} (glycine-alanine-glycine linkage) implies the increase/decrease of crystalline structure [17], which will be discussed in the subsequent XRD analysis section.

Titania sols can affect the spectra of silk fabrics. When silk fabrics are treated with titania sols (Fig. 1c, d, e, f), broadened absorption in the range of $800\text{--}400\text{ cm}^{-1}$ can be found. The weak peaks at 887 and 480 cm^{-1} indicate existence of $\text{Ti}\text{--}\text{O}\text{--}\text{Ti}$ bonds [18, 19]. Peaks around 995 and 967 cm^{-1} decrease obviously, while the peaks around $1,066$, $2,973$, and $2,927\text{ cm}^{-1}$ increase dramatically due to the introduction of BPET to silk fiber. BPET

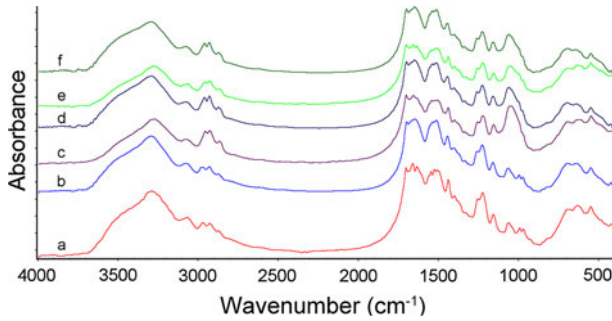


Fig. 1 FT-IR spectra of silk fabrics with different treatment. **a** Degummed silk fabric; **b** degummed silk fabric treated by COP; **c** degummed silk fabric first treated by TS, dried at 80 °C for 5 min, cured at 160 °C for 3 min, then treated by COP, washed (abbreviated as TC160); **d** degummed silk fabric first treated by COP, then by TS, dried at 80 °C for 5 min, cured at 140 °C for 5 min (abbreviated as CT140); **e** degummed silk fabric first treated by COP, then by TS, dried at 80 °C for 5 min, cured at 160 °C for 2 min (abbreviated as CT160); **f** degummed silk fabric first treated by COP, then by TS, dried at 80 °C for 5 min, cured at 170 °C for 1 min (abbreviated as CT170)

has a large molecule weight of 910.7 containing polar groups such as P–OH and Ti–OH (deviated from hydrolysis), which can react with amino or hydroxyl groups of silk fiber; meanwhile, BPET can hydrolyze and the resultants can react with the hydroxyl groups on the surface of titania network. As a result of these reactions, organic–inorganic hybrid blends (OIHBs) are formed on fiber surfaces [20, 21]. Scheme 2 shows the associating process between titania particles and silk fibers via titanate coupling agent BPET.

The wavenumber of newly introduced P–O–C in silk fiber is about $1,012\text{ cm}^{-1}$, and it may overlap with C–O–C strong vibration ($1,060\text{ cm}^{-1}$) leading to a much board, intensive peak between 930 and $1,130\text{ cm}^{-1}$. In order to confirm this hypothesis, we deconvoluted the three peaks respectively in Fig. 1a, b, and c near $1,066\text{ cm}^{-1}$ utilizing peakfit software [22]. Figure 2 shows two of the deconvolutions. All results reveal that each peak contains 3 hidden peaks: (1) approximately $1,060\text{ cm}^{-1}$, stretching vibration of C–O–C; (2) approximately 970 cm^{-1} , glycine-alanine-glycine linkage; (3) approximately $1,010\text{ cm}^{-1}$, stretching vibration of P–O–C. The wavenumbers of P–O–C are in accordance with many other researches [23, 24].

Curing conditions have important influences on the association between titania and silk fibers (see CT140, CT160 and CT180). With the increases of curing temperatures, more titania particles occur during the stages of soft and hard agglomeration between small

Scheme 2 Formation of OIHBs between silk fiber and nano-TiO₂ by BPET

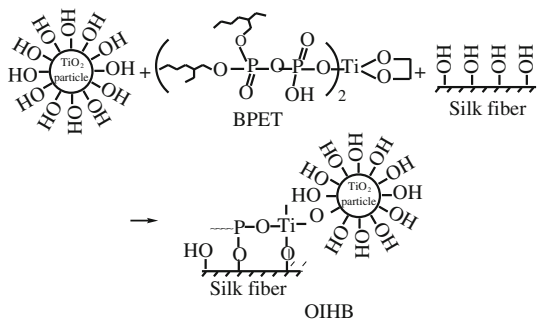
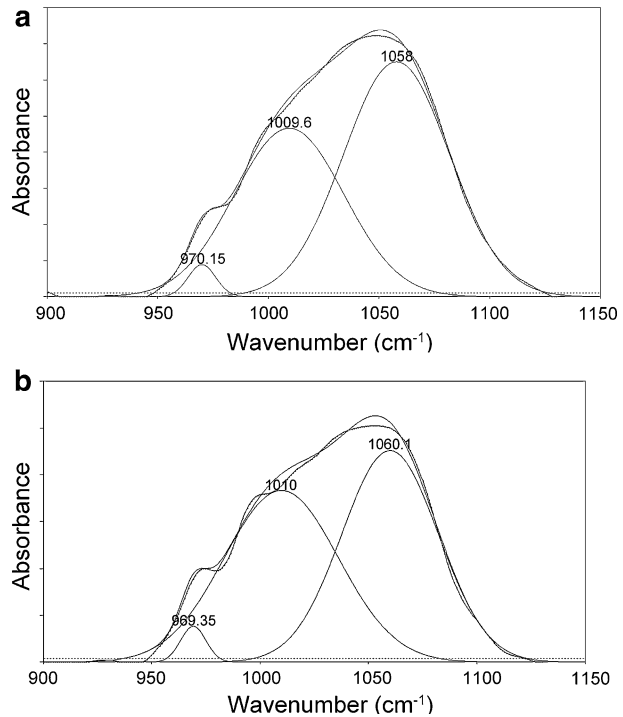


Fig. 2 Deconvolution of FT-IR peaks between wavenumber of 930–1,130 cm^{-1} in *B. mori* silk fabrics (**a** TC160; **b** CT180.)



nano-titania particles, and they are fixed on fiber surface by BPET. This will be further proved by FE-SEM images in the succeeding section.

XRD Analysis

XRD patterns of degummed *B. mori* silk fabrics and COP/TSS treated fabrics are presented in Fig. 3. The peaks near $2\theta = 20.7^\circ$ (plane 210), 24.7° (plane 030) are characteristic peaks of *B. mori* silk fibers [17, 25]. In order to calculate the crystallinity index and crystallite size of each samples, we deconvoluted all XRD patterns utilizing peakfit software. Figure 4 shows the deconvoluting result of a typical sample, CT160. The baseline was corrected by 2D linear method, and the curve was smoothed by Savitsky–Golay function, with peak type of “Gaussian area” (As a matter of fact, most instrument response is Gaussian.) selected as fitting criterion (options of “vary shapes”, “add residuals” were also selected). Other settings in the software were as their defaults. The calculation was executed repeatedly until the maximum R^2 had been achieved (iteration equals seven). Crystallinity index and crystallite size of each sample were calculated according Eqs. 1, 2, and 3, respectively (see Table 1).

As we can see from Table 1, crystallinity index of silk fabrics treated by COP/TSS and calculated by area method are smaller than that of degummed samples, while the data calculated by height method appear either higher or lower than that of degummed silk. Considering the contributions of both amorphous and crystalline regions on the whole XRD spectrum, many researchers have pointed out that the area method with XRD pattern deconvolution is more accurate in calculating the crystallinity index of fibers [14, 26–28]. Decreases of crystallinity may be a result of breaking of polypeptide chains and

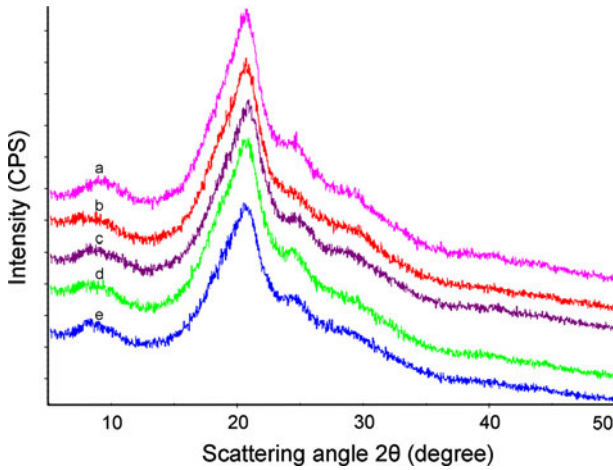


Fig. 3 XRD patterns of *B. mori* silk fabrics. **a** Degummed silk; **b** TC160; **c** CT140; **d** CT 160; **e** CT170

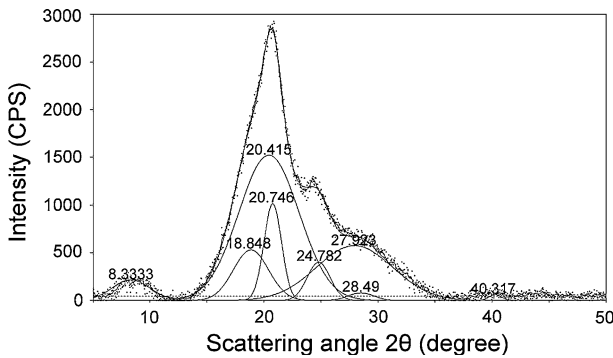


Fig. 4 XRD pattern deconvolution of *B. mori* silk fabric (CT160)

Table 1 Crystallinity index and crystallite sizes of *B. mori* silk fabrics

Samples	Crystallinity index (area)	Crystallinity index (height)	Crystallite size (nm)
Degummed silk	33.7	42.5	4.17
TC160	33.3	44.9	4.41
CT140	33.3	44.0	4.51
CT160	29.0	41.6	4.63
CT170	24.0	39.8	4.56

recombination of macromolecules in silk fibers during the plasma treatment [29]. The inner structure of silk fibers becomes looser, while crystallite size becomes larger. Like other textile fibers, *B. mori* silk fiber has both crystalline regions and amorphous regions. The amorphous regions have lower density and less order than crystalline regions. Crystalline regions can be partly oxidized or decomposed by etching roles of plasma. If titania sols was applied before COP treatment on silk fiber (sample of TC160), the OIHBS would

restrict the subsequent etching action of plasma on fiber surfaces, bringing about slightly decrease of crystallinity.

Curing conditions have important effects on the crystallinity of silk fiber. Higher curing temperatures or longer curing time can etch surfaces of large crystals or destroy some small crystals thus decrease the crystallinity of silk fibers. However, high curing temperature benefits the formation of nano-titania particles (sample of CT170). The characteristic peaks of nano-titania are not obviously distinguishable in all XRD patterns due to the fact that peaks are overlapped with some peaks of the *B. mori* silk fibers, or the curing temperature for massive formation of titania is still too low, leading to a content of nano-TiO₂ too low to be detected [30].

TG–DTA Analysis

Figure 5 presents the thermal characteristics of *B. mori* silk fabrics with detailed features of each curve listed in Table 2. The degummed silk fabric (Fig. 5a) has three mass loss processes:

(1) 30–214°C, which is assigned to the loss of absorbed moisture of silk fabric and a small amount of protein degradation, with mass loss of 11.2%; (2) 214–402°C, which is attributed to silk fabric decomposed into small molecules such as CO₂, H₂O, and other flammable substances, the major decomposition stage with mass loss of 40.9%; (3) 402–600 °C, which is mainly caused by char decomposition of silk fabric, with mass loss of 27.4%.

The pyrolysis of silk fiber is complicated and still unknown. The initial decomposition temperatures (T_{ini}) and the maximum decomposition temperature (T_{max}) can be determined precisely in the differential TG curves (DTG, not included in this paper). T_{ini} responds to the temperature at which the curve started dropping, while T_{max} responds to the temperature peak in the DTG curve [31].

Compared with degummed silk fabric (Fig. 5a), T_{ini} of COP/TSS treated samples are much higher. This is because the application of titania sols has improved the thermal stabilities of silk fabrics. Titania particles, and titanate coupling agent may diffuse into

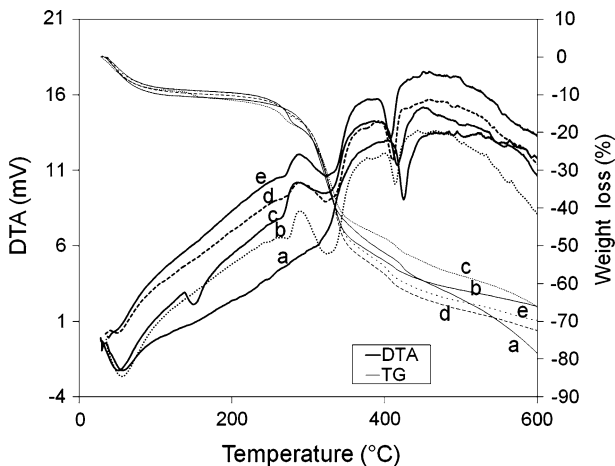


Fig. 5 TG–DTA of *B. mori* silk fabrics. **a** Degummed silk fabric; **b** TC1160l **c** CT170; **d** CT160; **e** CT140

Table 2 Thermal analysis data from TG–DTA curves of silk fabrics

Samples	T_i (°C)	T_{max} (°C)	Char residue at 600 °C (%)	Different mass loss stages		
				Temperature range (°C)	Mass loss (%)	Main peak temperature on DTA curve (°C)
Degummed silk	214	328	20.5	30–214	11.2	65
				214–402	40.9	–
				402–600	27.4	426
TC160	240	337	33.6	30–240	10.2	60
				240–389	42.4	280, 330
				389–600	13.8	414
CT140	237	338	30.0	30–237	10.1	54
				237–389	43.0	277, 331
				389–600	16.9	410
CT160	242	337	27.4	30–242	10.0	60
				242–373	43.2	272, 326
				373–600	19.3	441
CT170	249	334	33.1	30–249	12.7	64, 166
				249–368	31.8	277, 334
				368–600	22.3	419

amorphous regions of silk fiber, simultaneously, their hydroxyl groups can interact and dehydrate with those in the fiber forming covalent bonds, chemically or mechanically enhancing the thermal stabilities of amorphous region. T_{ini} of silk fibers treated by TSs were relatively high, which could be explained by XRD analysis results. Decreases of crystallinity index indicate that more amorphous regions occur in silk fibers treated by TSs, which allows more nano-particles or OIHBs of thermal stability penetrate into these regions, finally improves the initial decomposition temperature.

If titania sol applied first, the OIHBs will hinder the potential damage of plasma and thermal treatment on silk fiber, so the initial decomposition temperature will be improved. The fact that T_{ini} of TC160 is much higher than that of CT160 demonstrates this deduction. Increase of the curing temperature accelerates formation of nano-TiO₂ particles and OIHBs, which can penetrate into the amorphous region of silk fiber and improve the thermal stabilities.

The temperatures of maximum mass loss increase when silk are treated by COP/TSs. Higher percentages of char residue of the silk fabric treated with COP/TSs are due to the formation of OIHBs, which delays formation of more non-flammable char residue. The endothermic peaks around 279 °C are the results of the thermal decomposition of SF in unoriented silk II. The endothermic peaks of DTA curves in Fig. 5c are corresponding to the desorbing of moisture (about 60 °C) and heat absorption for degradation of silk fabric (330 °C). The new peak at 140 °C of CT170 indicates loss of absorbed moisture, because the short curing time of 1 min cannot sufficiently elevate surface temperature of fabric high enough to remove most of absorbed moisture or water from aggregation of titania. During the decomposing process of *B. mori* silk fiber, removal of CO₂ occurs over a narrow temperature scale (ca.350–500 °C), and then the two-step weight loss could be seen. As endothermic peaks on the DTA curves, the first peak near 370 °C, and the second peak near 410 °C can be found.

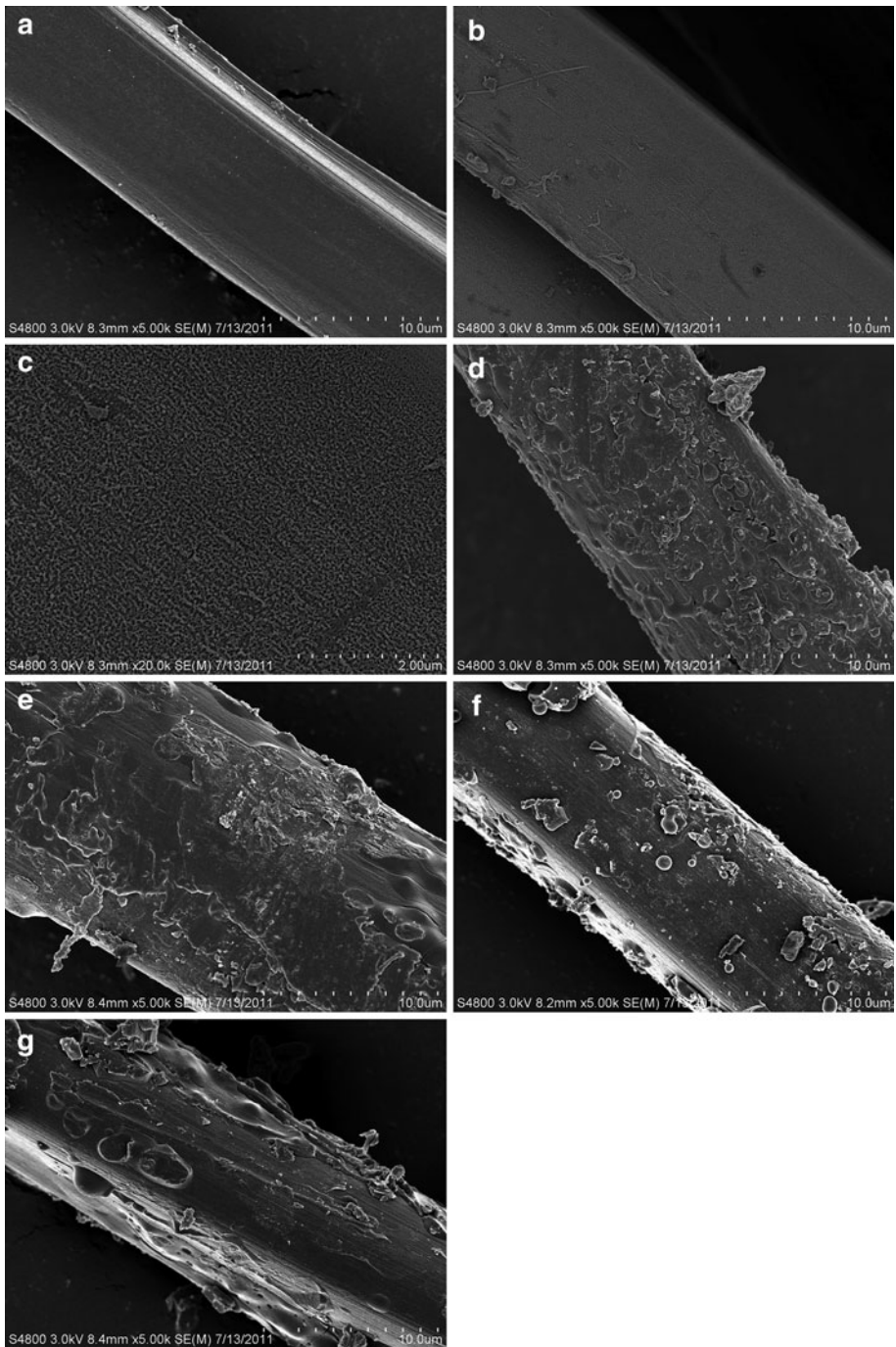


Fig. 6 SEM of *B. mori* fibers. **a** Degummed silk; **b** degummed silk after COP treatment (10 micron); **c** degummed silk after COP treatment (2 micron); **d** TC160; **e** CT140; **f** CT160; **g** CT170

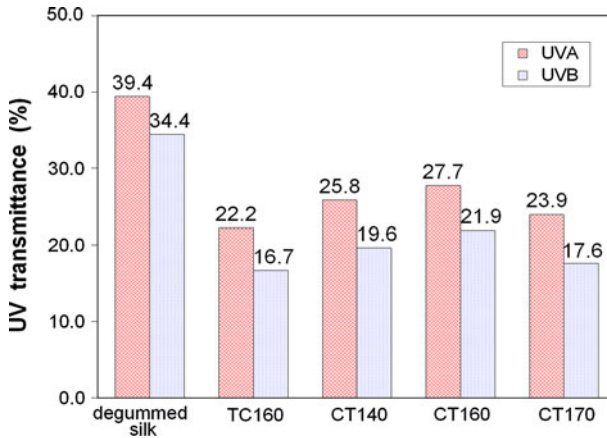


Fig. 7 UV transmittance of *B. mori* fabrics

SEM Analysis

Surfaces of *B. mori* silk fibers were investigated by FE-SEM with the results presented in Fig. 6. The surfaces of degummed silk fibers (Fig. 6a) are very smooth, with some mechanical scratches caused in the degumming process. Plasma can modify degummed silk fiber with different smoothness and micro-cavities (Fig. 6b, c). Application of plasma before titania sols treatment (Fig. 6e, f, g) is beneficial to form a much smooth surface. Surface of TC160 (Fig. 6d) is more coarse than that of CT160 since plasma treatment after application of titania sols will etch the OIHs seriously, leaving many tiny cavities in the layer.

Raising curing temperature (Fig. 6g) can promote both formation of nano-titania particles and better association between silk fiber and titania particles via coupling agent. So transparent layers of OIHs can be easily found on the surface of CT170.

UV Transmittance Analysis

UV transmittance of degummed and other treated *B. mori* silk fabrics were measured with the results presented in Fig. 7. The smaller the number becomes, the better UV resistance the fabric behaves. All samples treated by titania sols have good UV resistance [32]. When TSs are applied before COP treatment, more titania particles or OIHs occur because of the high energy and oxidation of oxygen plasma. Much UV radiation is reflected, refracted, or scattered so that less UV radiation can penetrate through fabrics. The mechanism of low UV transmittance in higher temperature cured samples is similar to that in oxidation of oxygen plasma.

Conclusions

Degummed *B. mori* silk fabrics modified by cold oxygen plasma and titania sols were investigated by FT-IR, XRD, TG-DTA, FE-SEM and UV transmittance methods, etc. FT-IR demonstrated that titania particles were associated with *B. mori* silk fiber forming OIHs. Processing sequence of COP and TSs, and curing conditions had significant

impacts on the crystalline, thermal, UV resistant characteristics of silk fabrics. Either applying TSs before COP treatment or curing at lower temperature was beneficial to obtain higher crystallinity index, less stable thermal ability, and lower UV transmittance, etc. FE-SEM analysis revealed that titania particles were adhered on fiber surfaces with different smoothness.

Acknowledgments The financial supports by National Natural Science Foundation of China (No. 50973079), Natural Science Foundation of Jiangsu Province (No. BK2010254) and a Project Funded by the Priority Academic Program Development of Jiangsu Higher Education Institutions are greatly appreciated. The authors of this paper would also like to thank Ms Qingqing Zhou, Ms Jingchun Lv from Textiles and Clothing Experimental Center of Yancheng institute of technology, Mr. Ning Qi, Mr. Dake Qin from National Engineering Laboratory for Modern Silk, Soochow University for their efforts in testing specimens.

References

- Ferrero F, Periolatto M, Burelli S, Carletto R (2010) Silk grafting with chitosan and crosslinking agents. *Fiber Polym* 11(2):185–192. doi:10.1007/s12221-010-0185-7
- Amiraliyan N, Nouri M, Kish M (2009) Electrospinning of silk nanofibers. I. An investigation of nanofiber morphology and process optimization using response surface methodology. *Fiber Polym* 10(2):167–176. doi:10.1007/s12221-009-0167-9
- Chen Y, Lin H, Ren Y, Wang H, Zhu L (2004) Study on *Bombyx mori* silk treated by oxygen plasma. *J Zhejiang Univ Sci* 5(8):918–922
- Inbakumar S, Anu Kaliani A (2010) Effect of plasma treatment on surface of protein fabrics. *J Phys Conf Ser* 208(1):012111
- Chan CM, Ko TM, Hiraoka H (1996) Polymer surface modification by plasmas and photons. *Surf Sci Rep* 24(1–2):1–54. doi:10.1016/0167-5729(96)80003-3
- Chu PK, Chen JY, Wang LP, Huang N (2002) Plasma-surface modification of biomaterials. *Mater Sci Eng R* 36(5–6):143–206. doi:10.1016/s0927-796x(02)00004-9
- Kim KS, Ryu CM, Park CS, Sur GS, Park CE (2003) Investigation of crystallinity effects on the surface of oxygen plasma treated low density polyethylene using X-ray photoelectron spectroscopy. *Polymer* 44(20):6287–6295. doi:10.1016/s0032-3861(03)00674-8
- Akbarzadeh R, Umbarkar SB, Sonawane RS, Takle S, Dongare MK (2010) Vanadia-titania thin films for photocatalytic degradation of formaldehyde in sunlight. *Appl Catal A Gen* 374(1–2):103–109.
- Nazari A, Montazer M, Rashidi A, Yazdandshenas M, Anary-Abbasinejad M (2009) Nano TiO₂ photocatalyst and sodium hypophosphite for cross-linking cotton with poly carboxylic acids under UV and high temperature. *Appl Catal A* 371(1–2):10–16. doi:10.1016/j.apcata.2009.08.029
- Abbasi AR, Morsali A (2010) Formation of silver iodide nanoparticles on silk fiber by means of ultrasonic irradiation. *Ultrason Sonochem* 17(4):704–710. doi:10.1016/j.ultsonch.2010.01.002
- Zubieta CE, Soltero - Martínez JFA, Luengo CV, Schulz PC (2011) Preparation, characterization and photoactivity of TiO₂ obtained by a reverse microemulsion route. *Powder Technol* 212(3):410–417. doi:10.1016/j.powtec.2011.06.017
- Zheng C, Chen G, Qi Z (2011) Ultraviolet resistant/antiwrinkle finishing of cotton fabrics by sol-gel method. *J Appl Polym Sci* 122(3):2090–2098. doi:10.1002/app.34289
- Zhang Y-Q, Shen W-D, Xiang R-L, Zhuge L-J, Gao W-J, Wang W-B (2007) Formation of silk fibroin nanoparticles in water-miscible organic solvent and their characterization. *J Nanopart Res* 9(5):885–900. doi:10.1007/s11051-006-9162-x
- Park S, Baker J, Himmel M, Parilla P, Johnson D (2010) Cellulose crystallinity index: measurement techniques and their impact on interpreting cellulase performance. *Biotechnol Biofuels* 3(1):10
- Min B-M, Jeong L, Lee KY, Park WH (2006) Regenerated silk fibroin nanofibers: water vapor-induced structural changes and their effects on the behavior of normal human cells. *Macromol Biosci* 6(4):285–292. doi:10.1002/mabi.200500246
- Suzuki E (1967) A quantitative study of the amide vibrations in the infra-red spectrum of silk fibroin. *Spectrochim Acta A Mol Spectrosc* 23(8):2303–2308. doi:10.1016/0584-8539(67)80123-5
- Lu Y, Lin H, Chen Y, Wang C, Hua Y (2007) Structure and performance of *Bombyx mori* silk modified with nano-TiO₂ and chitosan. *Fiber Polym* 8(1):1–6. doi:10.1007/bf02908152

18. Arier ÜÖA, Tepehan FZ (2011) Controlling the particle size of nanobrookite TiO₂ thin films. *J Alloys Compd* 509(32):8262–8267. doi:[10.1016/j.jallcom.2011.05.112](https://doi.org/10.1016/j.jallcom.2011.05.112)
19. Vasconcelos D, Eduardo N, Antônio S, João DC, Wander V (2011) Structural characterization and corrosion behavior of stainless steel coated with sol-gel titania. *J Mater Eng Perform* 20(3):1–7. doi:[10.1007/s11665-011-9919-y](https://doi.org/10.1007/s11665-011-9919-y)
20. Nakade M, Ichihashi K, Ogawa M (2005) Preparation of titania/PDMS hybrid films and the conversion to porous materials. *J Sol-Gel Sci Technol* 36(3):257–264. doi:[10.1007/s10971-005-4510-3](https://doi.org/10.1007/s10971-005-4510-3)
21. Hou A, Chen H (2010) Preparation and characterization of silk/silica hybrid biomaterials by sol-gel crosslinking process. *Mater Sci Eng B* 167(2):124–128. doi:[10.1016/j.mseb.2010.01.065](https://doi.org/10.1016/j.mseb.2010.01.065)
22. Pleshko N, Boskey A, Mendelsohn R (1991) Novel infrared spectroscopic method for the determination of crystallinity of hydroxyapatite minerals. *Biophys J* 60(4):786–793. doi:[10.1016/s0006-3495\(91\)82113-0](https://doi.org/10.1016/s0006-3495(91)82113-0)
23. DeLong HP, Edgewood Arsenal Aberdeen Proving Ground MD (1973) The infrared and raman spectra of isopropylmethylphosphonofluoridate (GB), Edgewood arsenal technical report, Edgewood Arsenal, Maryland, pp 1–13
24. Guan J, Chen G (2008) Flame resistant modification of silk fabric with vinyl phosphate. *Fiber Polym* 9(4):438–443. doi:[10.1007/s12221-008-0070-9](https://doi.org/10.1007/s12221-008-0070-9)
25. Magoshi J, Mizuide M, Magoshi Y, Takahashi K, Kubo M, Nakamura S (1979) Physical properties and structure of silk. VI. Conformational changes in silk fibroin induced by immersion in water at 2 to 130°C. *J Polym Sci Polym Phys Ed* 17(3):515–520. doi:[10.1002/pol.1979.180170315](https://doi.org/10.1002/pol.1979.180170315)
26. Segal L, Creely JJ, Martin AE, Conrad CM (1959) An empirical method for estimating the degree of crystallinity of native cellulose using the X-ray diffractometer. *Text Res J* 29(10):786–794. doi:[10.1177/004051755902901003](https://doi.org/10.1177/004051755902901003)
27. Teeäär R, Serimaa R, Paakkarl T (1987) Crystallinity of cellulose, as determined by CP/MAS NMR and XRD methods. *Polym Bull* 17(3):231–237. doi:[10.1007/bf00285355](https://doi.org/10.1007/bf00285355)
28. Garvey CJ, Parker IH, Simon GP (2005) On the Interpretation of X-ray diffraction powder patterns in terms of the nanostructure of cellulose I fibres. *Macromol Chem Phys* 206(15):1568–1575. doi:[10.1002/macp.200500008](https://doi.org/10.1002/macp.200500008)
29. Inbakumar S, Kaliani AA (2010) Effect of plasma treatment on surface of protein fabrics. *J Phys Conf Ser* 208(1):012111
30. Truijen I, Van Bael M, Rul H, D'Haen J, Mullens J (2007) Synthesis of thin dense titania films via an aqueous solution-gel method. *J Sol-Gel Sci Technol* 41(1):43–48. doi:[10.1007/s10971-006-0123-8](https://doi.org/10.1007/s10971-006-0123-8)
31. Ko J, Lee K, Bae D, Um I (2010) Miscibility, structural characteristics, and thermal behavior of wet spun regenerated silk fibroin/nylon 6 blend filaments. *Fiber Polym* 11(1):14–20. doi:[10.1007/s12221-010-0014-z](https://doi.org/10.1007/s12221-010-0014-z)
32. Rahal R, Pigot T, Foix D, Lacombe S (2011) Photocatalytic efficiency and self-cleaning properties under visible light of cotton fabrics coated with sensitized TiO₂. *Appl Catal B Environ* 104(3–4):361–372. doi:[10.1016/j.apcatb.2011.03.005](https://doi.org/10.1016/j.apcatb.2011.03.005)